J Mater Sci: Mater Electron (2013) 24:352–361
DOI 10.1007/s10854-012-0755-0

Role of diffusion-annealing time on the superconducting, microstructural and mechanical properties of Cu-diffused bulk MgB_2 superconductor

M. Dogruer · O. Gorur · Y. Zalaoglu · O. Ozturk · G. Yildirim · A. Varilci · C. Terzioglu

Received: 12 April 2012 / Accepted: 7 May 2012 / Published online: 20 May 2012

Abstract In this study, the effect of various annealing time (0.5, 1, 1.5 and 2 h) on microstructural, mechanical and superconducting properties of the Cu-diffused bulk MgB_2 superconducting samples is investigated using X-ray diffraction (XRD), scanning electron microscopy (SEM), Vickers microhardness (H_v) and dc resistivity measurements for the first time. The critical transition temperature, grain size, phase purity, lattice parameter, surface morphology, crystallinity and room temperature resistivity values of the bulk samples prepared are compared with each other. Electrical-resistivity measurements show that the sample (annealed at 850 °C for 1 h), exhibiting the highest room temperature resistivity, obtains the maximum zero resistivity transition temperature (T_c). From the XRD results, all the samples contain MgB_2 as the main phase with a very small amount of Mg_2Cu phase. Moreover, SEM investigations conducted for the microstructural characterization illustrate that not only does the grain size of the samples studied enhance gradually, but the surface morphology and grain connectivity also improve with the increase in the diffusion-annealing time up to 1 h beyond which all the properties obtained start to degrade. Indeed, the worst surface morphology is observed for the Cu-diffused bulk MgB_2 superconductor exposed to 2 h annealing duration. At the same time, Vickers microhardness, elastic modulus, load independent hardness, yield strength, fracture toughness and brittleness index values are calculated separately for the pure and Cu-diffused samples. It is found that the microhardness values depend strongly on the diffusion-annealing time. Furthermore, the diffusion coefficient of the Cu ion in the bulk MgB_2 superconductor is obtained to change from 1.63×10^{-7} to 2.58×10^{-7} $cm^2\ s^{-1}$. The maximum diffusion coefficient is observed for the sample prepared at 850 °C for 1 h whereas the minimum one is noted for the sample annealed at 850 °C for 2 h, confirming that the annealing-time of 1 h is the best ambient to improve the mechanical, microstructural and superconducting properties of the samples produced.

1 Introduction

Magnesium diboride (MgB_2) material, a simple binary superconductor at 39 K [1], exhibits the highest transition temperature among the inter-metallic compounds. MgB_2 material has been described as 1.5 type superconductor due to the fact that this material presents both the properties of type-I and type-II superconductors. Moreover, the MgB_2 superconductor, composed of two conduction bands and two superconducting gaps, is a unique superconductor for potential technological and industrial applications [2, 3] owing to the remarkably high critical temperature, high critical current density, large coherence length, low anisotropy, light weight, absence of weak–links and simple crystal structure properties around 20 K [4–6]. Thus, the MgB_2 superconductor in the forms of polycrystalline bulk, wire, tape and thin film is one of the most attractive

M. Dogruer · O. Gorur · G. Yildirim · A. Varilci · C. Terzioglu (✉)
Department of Physics, Abant Izzet Baysal University, 14280 Bolu, Turkey
e-mail: terzioglu_c@ibu.edu.tr

Y. Zalaoglu
Department of Physics, Osmaniye Korkut Ata University, 80000 Osmaniye, Turkey

O. Ozturk
Department of Physics, Kastamonu University, 37100 Kastamonu, Turkey

materials to investigate the superconductivity in two component superconductors.

Since the discovery of the MgB_2 superconductor materials, researchers have endeavored to improve its superconducting, electrical, mechanical, physical, microstructural and flux pinning properties to make them suitable for high temperature and magnetic field applications [7–9]. However, the preparation of the pure MgB_2 phase is a very difficult task due to the presence of several phases such as MgB_6, MgB_{12} and MgO during the phase formation [10–13]. A number of the preparation conditions such as the annealing ambient, composition, type and quantity of the dopant, heat-treatment method and operational procedures also affect the formation of the MgB_2 phase and the mechanical, microstructural, superconducting and flux pinning properties of them. Thus, scientists have tried to determine the best condition for the improvement of these properties in the MgB_2 material for many years. In our previous study [14], we examined the role of diffusion-annealing temperature on the microstructural and superconducting properties of the Cu-diffused bulk MgB_2 superconductor and found the improvement of the microstructural and superconducting properties of the samples with the increase in the diffusion-annealing temperature.

According to the literature research, no detailed work has been published on the mechanical, microstructural and superconducting properties of the Cu-diffused bulk MgB_2 sample in terms of the change in the diffusion-annealing time. In the present study, we investigate the effect of the annealing time on the microstructural and superconducting properties of the Cu-diffused MgB_2 bulk samples in detail by means of the scanning electron microscopy, Vickers microhardness, X-ray diffraction and dc resistivity measurements. Moreover, the microhardness, elastic modulus, yield strength, fracture toughness, brittleness index and ductility, which are the important parameters for industrial applications of the superconductor materials, are clearly discussed [15]. It is observed that the microstructural, superconducting and mechanical properties of the bulk MgB_2 superconductors are strongly dependent upon the diffusion-annealing time.

2 Experimental details

The starting material in this work is commercially available MgB_2 powder (Alfa Aesar, −325 mesh, <44 micron). At room temperature the precursor powder of 0.25 g is pressed into the rectangular pellets form in the size of 40×4 mm^2 under 350 MPa pressure to obtain 5 identical bulk samples. The fine samples produced are placed in a stainless steel tube and sintered at 850 °C for various time such as 0.5, 1, 1.5 and 2 h in tube furnace (Protherm-Model PTF12/75/200). During the annealing process, Argon gas atmosphere is maintained to be 5 bars in the steel tube and all the samples are cooled down to room temperature with the constant cooling rate of 5 °C min^{-1} in the furnace. Among them, 4 samples chosen are exposed to copper (Cu) diffusion process conducted by an AUTO306 vacuum coater (EDWARDS). The Cu-diffused bulk MgB_2 samples are sintered at 850 °C for 0.5, 1, 1.5 and 2 h and herein after denoted as Cu1, Cu2, Cu3 and Cu4, respectively. Likewise, the pure sample annealed at 850 °C for 1 h will be presented as Cu0.

The electrical property of the samples is investigated by dc resistivity versus temperature measurements using 5 mA dc current through the samples in the He gas contact cryocooler from CRYO Industries in the temperature range from 10 to 50 K. Both voltage and current contacts are made with silver glue contact. A Keithley 220 programmable current source and a Keithley 2182A nano-voltmeter system are used for the conventional four-probe measurements.

The phase and crystal structure of the Cu-diffused and pure samples are analyzed by means of a Rigaku Multiflex+ XRD 12 kW rotating anode powder X-ray diffractometer. The diffraction data are obtained from the diffraction angle in the range $3° \leq 2\theta \leq 90°$ at room temperature (300 K). The parameters measured are diffracted beam graphite (0002) monochromator, CuKα radiation ($\lambda = 1.5418$ Å), a tube voltage of 38 kV and a tube current of 30 mA, a step scan-size of 0.02°, with a counting time of 3 s per point. Phase purity and lattice parameters are evaluated from the XRD patterns. The accuracy in determining the lattice parameters (a and c) is ±0.0001 Å. Average grain size of the samples prepared is also found by the Scherrer–Warren approach [16, 17]. Further, the surface morphology and grain connectivity of the pure and Cu-diffused samples are studied by using scanning electron microscope (SEM) JEOL 6390-LV, operated at 20 kV in the secondary electron image (SEI) mode with a resolution power of 3 nm.

Vickers microhardness measurements are performed in air with the aid of a digital microhardness tester (Shimadzu HVM-2) at room temperature to characterize the mechanical properties of samples annealed at different duration. A rigid Vickers pyramidal indenter with various loads such as 0.245, 0.490, 0.980, 1.960 and 2.940 N is applied for a single loading time of 10 s and the diagonals of indentation are measured with an accuracy of ±0.1 μm. The Vickers microhardness values are determined with an average of 20 readings at different locations of specimen surfaces to obtain reasonable mean values for each load. All the results obtained for the Cu-diffused samples are compared with that for the pure sample.

3 Result and discussion

X-Ray diffraction analysis, Scanning electron microscopy, Vickers microhardness and resistivity measurements are used to determine the effect of diffusion-annealing time on the microstructural, mechanical and superconducting of the Cu-diffused bulk MgB_2 superconductors.

3.1 Electrical resistivity measurements

Dc electrical resistivity as a function of temperature is measured in the range from 10 to 50 K to examine the influence of Cu diffusion on superconducting properties of the samples and the results obtained are given in Fig. 1. As can be seen from the figure, all the samples show metallic behavior above the T_c value. Resistivity of the samples at room temperature (300 K) is listed in Table 1. It is apparent form the table that the resistivity value of the samples gradually increases from 62 to 129 μΩcm with the enhancement in the diffusion-annealing time up to 1 h beyond which the resistivity values start to decrease systematically to a local minimum (86 μΩcm) for the Cu4 sample. Moreover, the onset critical T_c^{onset} and offset critical T_c^{offset} temperature determined from the normalized resistance graphs (Fig. 2) are tabulated in Table 1. As seen from the table the offset and onset critical temperatures of the samples studied in this work are observed to be in a range of 38.1–39.3 K and 38.3–36.2 K, respectively. All the results obtained show that both T_c^{onset} and T_c^{offset} values regularly increase with ascending the diffusion-annealing time up to 1 h after which they decrease slowly; in fact, the minimum critical temperature values ($T_c^{\text{offset}} = 38.1$ and $T_c^{\text{onset}} = 36.2$ K) are obtained for the Cu4 sample as a result of the degradation of the crystallinity and connectivity between grains and decrement in the grain size. At the same time, the variation of $\Delta T_c = T_c{}^{\text{onset}} - T_c{}^{\text{offset}}$ is illustrated in Table 1. One can see from the table, the minimum ΔT_c is found to be about 1.0 K for the Cu2 sample whereas the maximum variation is obtained to be about 1.9 K for the Cu4 sample due to the grain misorientations and decrement of the crystallinity [18]. According to the findings of the resistivity survey, the duration of 1 h is determined to be the best annealing-time for the Cu-diffused bulk MgB_2 sample, which confirms that the annealing ambient (time, temperature, atmosphere and pressure) plays a very significant role on the superconducting, pinning mechanism, microstructural, mechanical, electronical and physical properties of the superconductor materials due to the contribution of the phonon subsystem and the electron–phonon anharmonicity described by the third rank polar tensors explaining the local non-centro symmetry contribution to the superconductor materials [19].

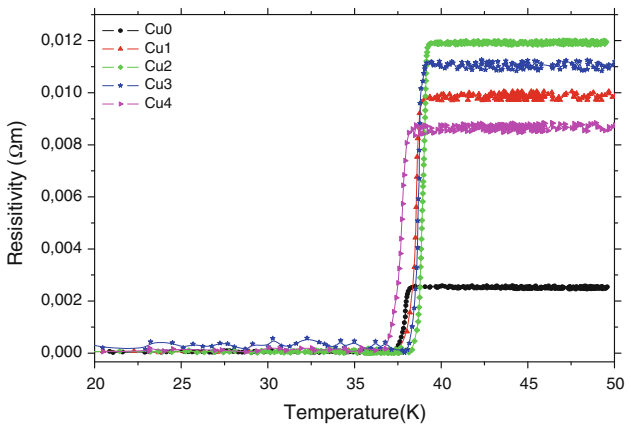

Fig. 1 Resistance versus temperature as a function of temperature *curves* for the samples

Table 1 Resistivity measurement results for the samples

Samples	T_c^{onset} (K)	T_c^{offset} (K)	ΔT_c (K)	Resistivity at 300 K (Ω m)
Cu0	38.4	36.9	1.5	0.0062
Cu1	38.8	37.5	1.3	0.0098
Cu2	39.3	38.3	1.0	0.0129
Cu3	39.2	38.0	1.2	0.0115
Cu4	38.1	36.2	1.9	0.0086

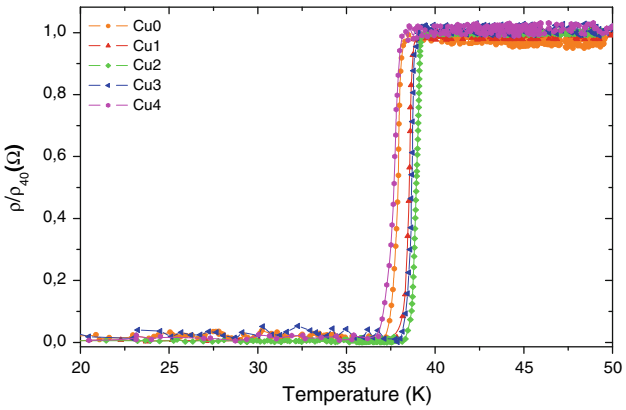

Fig. 2 Normalized resistivity as a function of temperature *curves* for the samples

3.2 XRD Analyses

The XRD patterns of the samples prepared are pictured in Fig. 3 where the corresponding (*h k l*) Miller indices belonging to MgB_2 main lines are also shown. As seen from the figure, the pure and Cu-diffused samples (except for the Cu4) contain the MgB_2 phase only and exhibit the polycrystalline superconducting phase. Moreover, the Cu2

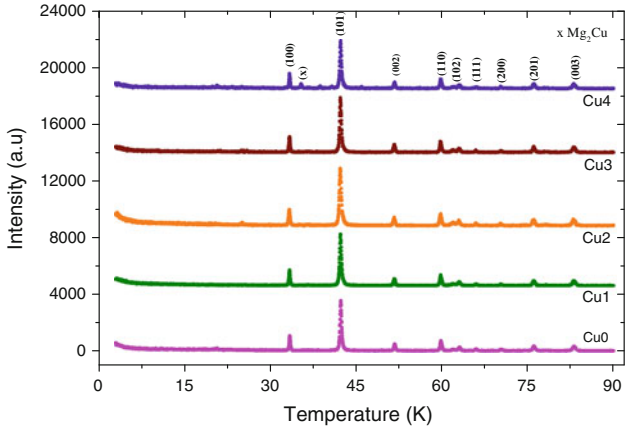

Fig. 3 XRD patterns of Cu0, Cu1, Cu2, Cu3 and Cu4

sample has the highest peak intensities belonging to the main phase of the MgB_2 diffraction patterns. According to the results, the best ambient is determined to be 850 °C for 1 h to obtain the formation of MgB_2 phase. On the other hand, the Cu4 sample has the Mg_2Cu phase formation as a result of the decomposition of the MgB_2 phase and rapid evaporation of Mg at 850 °C for 2 h [4]. In addition, the cell parameters a and c are calculated with respect to the hexagonal unit cell structure using the least square method through d value and (h k l) planes. The a and c parameters computed are depicted in Table 2. It is visible from the table that a systematic expansion in the a and c axis lengths is observed with ascending diffusion-annealing time until 1 h beyond which a regular contraction in the cell parameters is noticed for the samples, presenting that the Cu2 sample obtains the best crystallinity and grain connectivity. Additionally, the broadening nature of the XRD peaks reveals that the crystallite size of the samples is found to be within the nanometer scale by using the Scherrer–Warren equation [19–22]. In point of the Eq. (1), the average size of a crystal in the broadening region is defined as,

$$d = 0.941\lambda/B\cos\theta_B \quad (1)$$

where d is the thickness of the crystal, λ presents the wavelength, B denotes the full width half maximum (FWHM) of the Bragg peak corrected using the corresponding peak in micron-sized powder and θ_B is the Bragg angle. Also,

$$B^2 = B_m^2 - B_s^2 \quad (2)$$

where B_s denotes the half width of the standard material in radians. The grain size values obtained for the samples are displayed in Table 2. It is found that the Cu2 sample has the highest grain size (74 nm) whereas the crystallite size of 39 nm is the smallest value for the Cu4 sample, showing that the best crystal structure for the Cu-diffused MgB_2 superconductor is obtained at 850 °C for 1 h.

Table 2 XRD measurement results for the samples

Samples	Lattice parameter a (Å)	Lattice parameter c (Å)	Grain size (nm)
Cu0	3.0831	3.5193	55
Cu1	3.0847	3.5334	58
Cu2	3.0886	3.5345	74
Cu3	3.0856	3.5341	65
Cu4	3.0823	3.5303	39

3.3 SEM analyses

The surface morphology of the Cu-diffused MgB_2 samples is studied for the determination of the possible precipitation at the grain boundaries by Scanning Electron Microscopy (SEM) investigations. Figure 4 a–e depicts the SEM pictures (taken in the secondary electron image mode) of the surfaces of the Cu0, Cu1, Cu2, Cu3 and Cu4 samples, respectively. It is visible from the figure that the diffusion-annealing time affects the surface morphology. The microtructures of the Cu1, Cu2 and Cu3 samples are significantly different from that of the Cu0 and Cu4 samples. Among the samples, the Cu2 sample has the best surface morphology (densest and smoothest) and grain connectivity and lowest porosity. On the other hand, the grains in the Cu0 and Cu4 samples are randomly oriented and poorly connected (Fig. 4). In fact, the latter obtains the non-uniform surface appearance with smaller grains. Based on these results, the surface morphology is found to improve with the increment in the diffusion-annealing time until 1 h beyond which the grain connectivity is observed to degrade, confirming that the quality of the microstructure depends strongly on the annealing duration.

3.4 Calculation of diffusion coefficient

As well known several methods are studied for the estimation of the diffusion parameter in polycrystalline high-T_c superconductors [14, 21]. In this paper, the diffusion coefficients of Copper (Cu) ions in the bulk MgB_2 superconductors prepared at 850 °C for different annealing-time such as 0.5, 1, 1.5 and 2 h are calculated for the first time. Here, the coefficients are found by means of the resistivity measurements of the samples after the successive removal of thin layers on the samples studied. It is argued that the conditions of impurity diffusion from a constant source into a semi-infinite solid can be defined by following equation [23, 24]:

$$N(x,\ t)\ =\ N_0$$

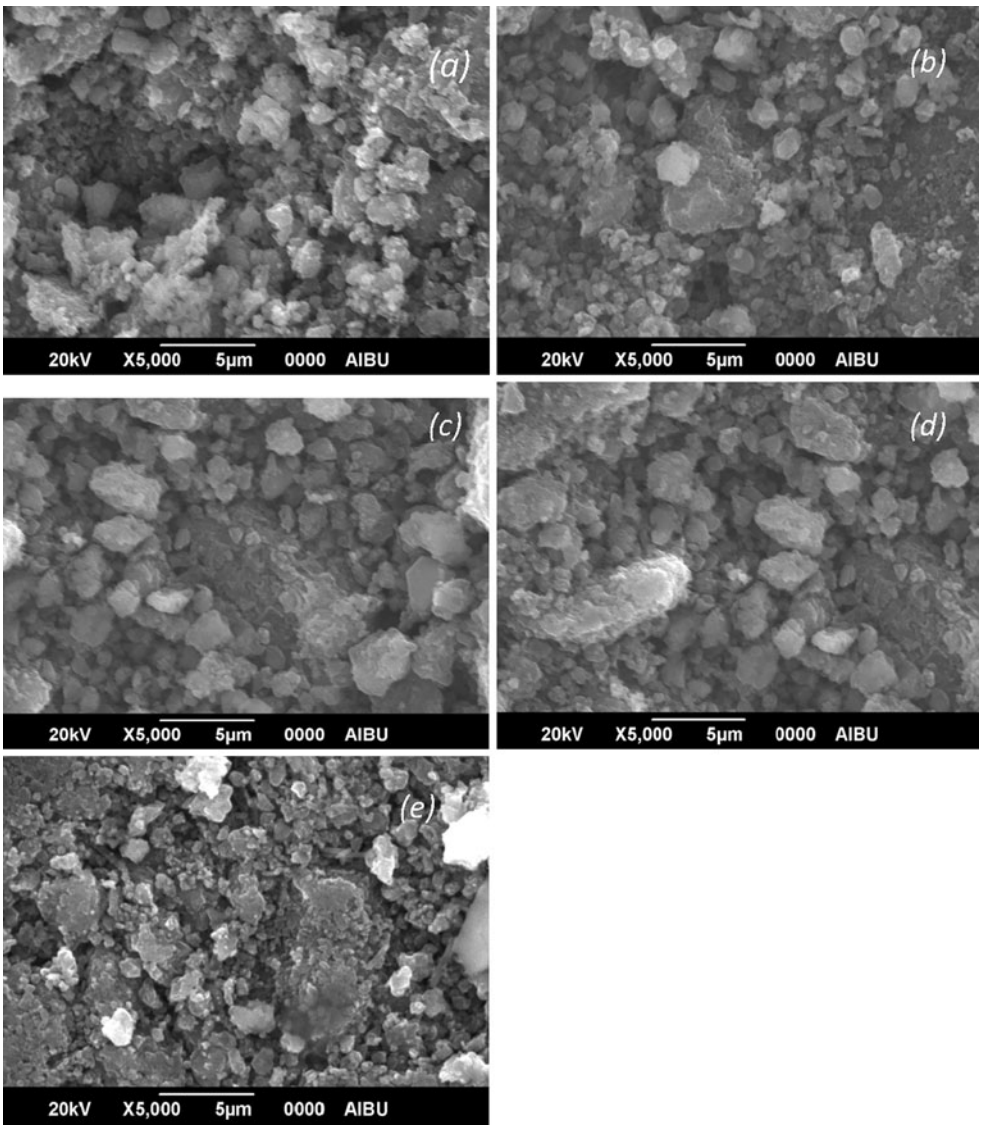

Fig. 4 SEM micrographs of **a** Cu0, **b** Cu1, **c** Cu2, **d** Cu3 and **e** Cu4

$$\left[1 - \mathrm{erf}\left(x/2\sqrt{Dt}\right)\right] \tag{3}$$

where erf $[x/2(Dt)^{1/2}]$ displays the error function with argument $y = \left[x/2\sqrt{Dt}\right]$

$$\mathrm{erf}(y) = \left(2/\sqrt{\pi}\right) \int_0^y \mathrm{erf}(-y^2) \tag{4}$$

where $N_0 = N(0, t)$ is the constant concentration on the surface of the sample, N(x, t) presents the impurity concentration at the distance x from the surface, D shows the diffusion coefficient and t denotes the diffusion-annealing time. The equations given give that the resistivity (ρ) with thickness of the sample studied is similar to the concentration distribution of the diffused impurity. Figure 5 exhibits the variation of resistivity $\Delta\rho/\rho_0$ (ρ_0 denotes the resistivity of the pure region of the sample) as a function of thickness of the samples produced. The solid curve reveals the calculated concentration profile of Cu in the bulk MgB_2 sample. As seen from the figure the experimental data obtained fit well with the theoretical curve, and the diffusion coefficients calculated by using Eq. (3) are found to be about 6.32×10^{-7}, 9.48×10^{-7}, 8.22×10^{-7} and 3.57×10^{-7} cm^2 s^{-1} for the Cu1, Cu2, Cu3 and Cu4 samples, respectively. According to these results, the diffusion coefficient of the copper varies with the annealing time, and the annealing duration of 1 h is much more significant compared to the others, showing that the Cu diffusion in the bulk MgB_2 superconductor depends strongly on the diffusion-annealing time.

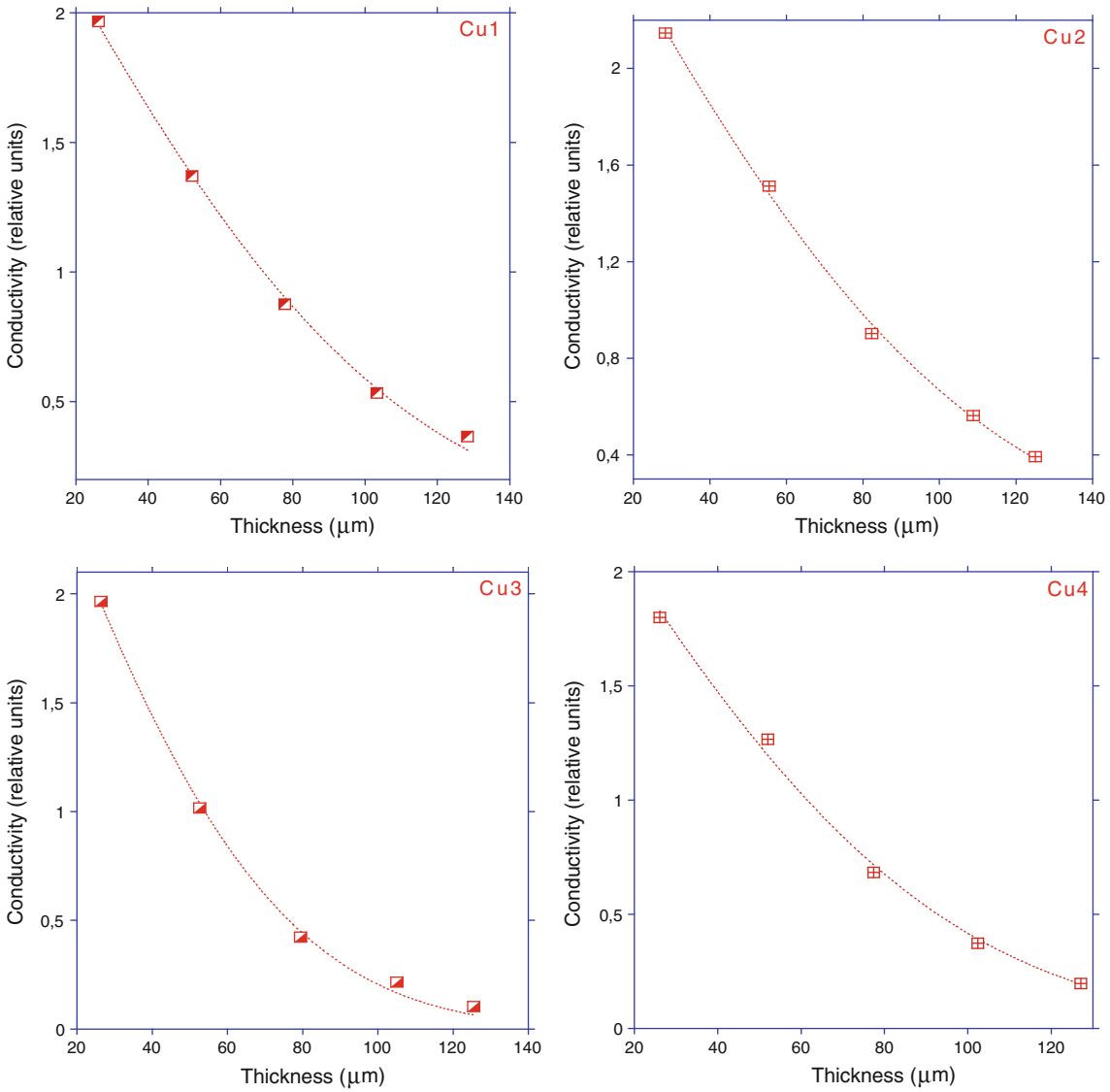

Fig. 5 Concentration profile of Cu over the thickness of the samples exposed to Cu diffusion for 0.5, 1, 1.5 and 2 h

3.5 Vickers microhardness measurements

The diagonal length as a function of test load is measured to describe the effect of Cu-diffusion on mechanical properties of the samples prepared in this work. As well known, standard Vickers microhardness measurements consist of a load (F) on the test material through geometrically defined indenter and after the indenter is removed, measuring the characteristic dimension (d) of the resultant impression.

The Vickers microhardness values of different applied loads in the range from 0.245 to 2.940 N are calculated by means of the following equation,

$$H_V = 81.9635\left(\frac{F}{d^2}\right) \quad \text{(GPa)} \tag{5}$$

where H_v denotes the Vickers hardness, d (in μm unit) is diagonal length of indentation and F presents the applied load in Newton. The Vickers hardness (H_v), elastic modulus (E), yield strength (Y), fracture toughness (K_{IC}) and brittleness index (B) calculated with the aid of Eqs. 5–8 [25, 26] are listed in Table 3.

$$E = 81.9635H_V \tag{6}$$

$$Y \approx \frac{H_V}{3} \tag{7}$$

Table 3 The calculated load dependent Hv, E, Y, K_{IC} and B for the samples

Samples	Load (N)	d (μm)	H_v (GPa)	E (GPa)	Y (GPa)	K_{Ic} (Pa/m$^{1/2}$)	B (μm$^{1/2}$)
Cu0	0.245	14.09	2.288	187.57	0.762	2.411	0.948
	0.490	23.50	1.644	134.78	0.548	2.044	0.804
	0.980	37.04	1.325	108.56	0.441	1.834	0.722
	1.960	62.03	0.945	77.42	0.314	1.549	0.610
	2.940	85.20	0.751	61.55	0.250	1.381	0.543
Cu1	0.245	13.87	2.361	193.56	0.787	2.208	1.069
	0.490	22.78	1.751	143.52	0.583	1.901	0.921
	0.980	34.10	1.562	128.06	0.520	1.796	0.869
	1.960	56.98	1.119	91.75	0.373	1.520	0.736
	2.940	70.32	1.102	90.36	0.367	1.508	0.730
Cu2	0.245	9.15	5.423	444.55	1.807	4.310	1.258
	0.490	14.21	4.496	368.52	1.498	3.924	1.145
	0.980	23.39	3.320	272.17	1.106	3.372	0.984
	1.960	38.67	2.429	199.16	0.809	2.885	0.841
	2.940	47.64	2.402	196.88	0.800	2.868	0.837
Cu3	0.245	12.67	2.830	231.97	0.943	2.398	1.180
	0.490	20.43	2.175	178.33	0.725	2.102	1.034
	0.980	31.57	1.823	149.45	0.607	1.925	0.947
	1.960	48.14	1.568	128.54	0.522	1.785	0.878
	2.940	62.01	1.417	116.21	0.472	1.697	0.835
Cu4	0.245	16.19	1.733	142.06	0.577	2.001	0.866
	0.490	30.61	0.969	79.46	0.323	1.496	0.647
	0.980	56.57	0.567	46.53	0.189	1.145	0.495
	1.960	100.45	0.360	29.52	0.120	0.912	0.394
	2.940	133.23	0.307	25.17	0.102	0.842	0.364

$$K_{IC} = \sqrt{2E\gamma} \quad (\gamma,\ \text{surface energy}) \tag{8}$$

$$B = \frac{H_v}{K_{IC}} \tag{9}$$

The variation of microhardness as a function of the applied load for all the samples is displayed in Fig. 6. It is obvious from the figure that the microhardness values are strongly dependent upon the Indentation load (ISE, indentation size effect) and diffusion-annealing time. The Vickers microhardness values obtained are depicted in Table 3. As seen from the table, the microhardness values change from 0.307 to 2.402 GPa at the constant load of 2.940 N for the samples produced. The microhardness value of 2.402 GPa is found to be the maximum for the Cu2 sample whereas the minimum value (0.307 GPa) is obtained for the Cu4 sample. Moreover, the elastic modulus, yield strength, fracture toughness and brittleness index values deduced from the Vickers microhardness measurements enhance with the increment in the diffusion-annealing time up to 1 h beyond which these values start to decrease, in fact the Cu4 sample has the smallest values (Table 3) as a result of the distortion in the bond strength of the sample and more porous structure [27], supported by the SEM images (see Fig. 4).

The change in the microhardness values is noticed with increasing the applied load from 0.245 to 2.000 N only due to the weakness grain boundaries [27]. Moreover, Fig. 4 shows that the Vickers microhardness values are load dependent for the samples and the microhardness values calculated decrease non-linearly as the applied load increases up to 2 N

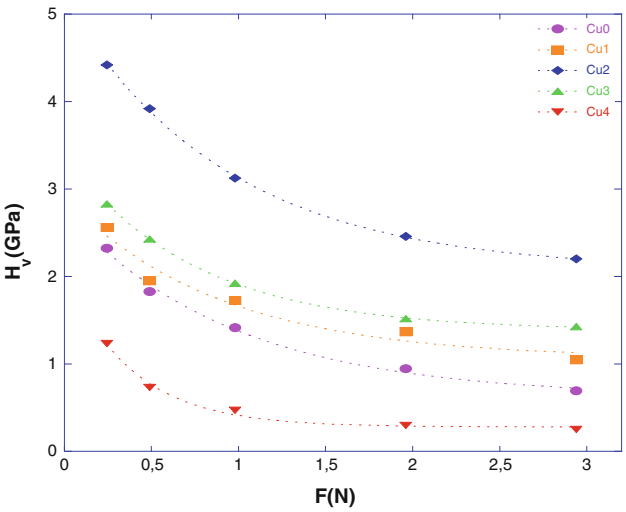

Fig. 6 The variations of microhardness with load for the samples

beyond which the curves shift to the saturation (plateau) region. This non-linearity known as ISE can be seen in the literature [28, 29]. It is apparent from Table 3 that the calculated microhardness values of the Cu2 sample are higher than the other samples as a result of better crystallinity and connectivity between grains, supported by the XRD and SEM findings.

There are two different methods to describe the load dependence of a sample: elastic portion and energy dissipative processes. According to the former method, the indentation includes an elastic portion. The elastic part of the deformation is relaxed on unloading, which can be accounted for by adding an elastic component (d_e) to the measured plastic indentation semidiagonal (dp). Hence the true hardness value (H_0) can be found by the following formula [30]:

$$H_0 = 1854.4\left\lfloor \frac{F}{(d_p + d_e)^2} \right\rfloor \tag{10}$$

From the Eq. (10), the indentation diagonals measured are linear with the square root of the applied load, and the slope of such a curve is proportional to $(H_0)^{1/2}$. Additionally, the vertical intercept of the curve directly gives the elastic part of the indentation semidiagonal (d_e) [26]. Moreover, Fig. 7 indicates the applied load dependence of the indentation diagonals examined by means of d_p versus $F^{1/2}$ plots. H_0, d_e and LRC (linear regression coefficients) values evaluated from Fig. 7 are also depicted in Table 4. Like the Vickers microhardness results, the H_0 values initially increase with the enhancement in the diffusion-annealing time up to 1 h, but they start to reduce abruptly.

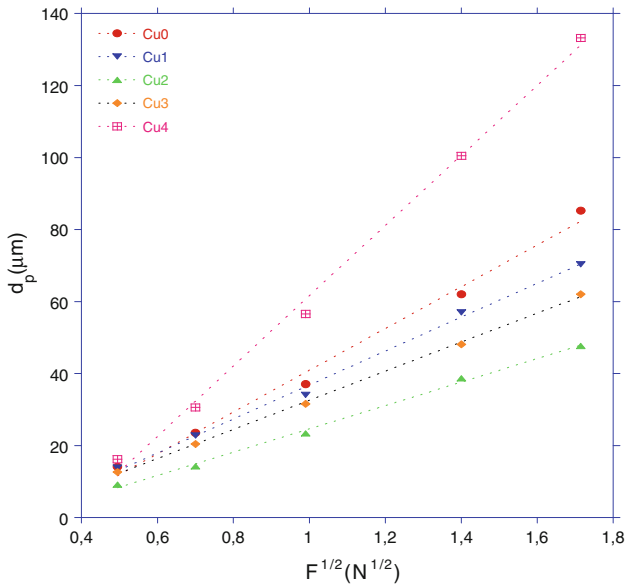

Fig. 7 *Plots* of diagonal length versus square root of applied loads for the samples

On the other hand, the *de* values computed regularly decrease with the increment in the diffusion-annealing time.

Moreover, in literature it is indicated that the hardness–load curve exhibits distinct transition (associated with the intrinsic hardness value of the material) to a plateau of constant hardness [31], and the H_0 values are nearly close to the experimentally estimated H_v values in the plateau region [32]. In this study, the plateau (saturated) region is reached at 2 N applied load for the samples studied. From the Table 4, the true microhardness value of the Cu2 sample (1.754 GPa) is smaller than the hardness results (see Table 3) in plateau region ($H_v = 2.402$ and 2.429 GPa). This behavior can also be seen for the other samples. In other words, the true hardness values of all the samples are smaller than conventionally calculated ones. Based on the results, the elastic portion method is not suitable for the determination of the microhardness values for the Cu-diffused bulk MgB_2 superconductors due to the difference between the calculated results and true hardness values [33].

The second method considers the energy dissipative processes rather than the elastic processes during the indentation. According to the former model, a true microhardness defined by subtracting a dissipative part F_0 from the applied load can be described by using following equation [33]:

$$H_v = 1854.4\left(\frac{F - F_0}{d^2}\right) \quad \text{(GPa)} \tag{11}$$

The variation of the applied load inferred from the square of the impression semidiagonal length is pictured in Fig. 8. When the slope of each line coincides with the load independent hardness constant (H_0), the vertical intercept of each line exhibits the sample resistance pressure (F_0). As can be seen from the figure, all the samples studied indicate the excellent linear relationship. The values of F_0 and H_0 are calculated via the Eq. (11). The F_0, H_0 and *LRC* values obtained are listed in Table 5. One can see from the table, the H_0 values obtained reduce with the enhancement in the diffusion-annealing time up to 1 h beyond which the values are found to increase and the maximum point is observed for the Cu4 sample. On the other hand, the change of the

Table 4 Best-fit results of experimental data according to Eq. 10

Samples	H_0 (GPa)	d_e (μm)	LRC	H_v (GPa)
Cu0	0.551	17.08	0.9956	0.751–0.945
Cu1	0.835	10.31	0.9983	1.102–1.119
Cu2	1.756	7.78	0.9984	2.402–2.429
Cu3	1.139	7.82	0.9996	1.417–1.568
Cu4	0.195	35.9	0.9980	0.307–0.360

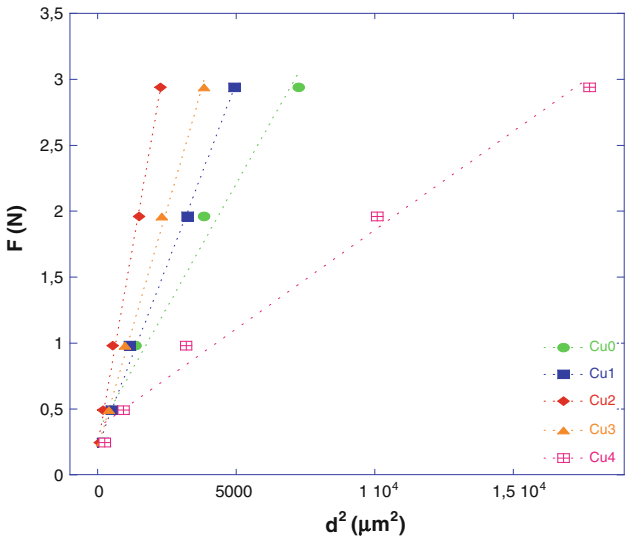

Fig. 8 *Graph* of applied load against the square of the diagonal length for the samples

Table 5 Best-fit results of experimental data according to Eq. 11

Samples	H_0 (GPa)	F_0 (N)	LRC	H_v (GPa)
Cu0	0.696	0.328	0.9905	0.751–0.945
Cu1	1.021	0.214	0.9976	1.102–1.119
Cu2	2.208	0.227	0.9980	2.402–2.429
Cu3	1.351	0.195	0.9982	1.417–1.568
Cu4	0.277	0.357	0.9942	0.307–0.360

resistance pressures is randomly found in the samples produced.

According to the experimental observations, the diagonal length is obtained to be exactly dependent on the applied load. This expression can be explained using the following equation [34]:

$$\frac{F}{d} = H_0 d + \gamma \tag{12}$$

Figure 9 reveals that how we fit the *F*/*d* versus diagonal length of indentation (*d*) for all samples. As seen from the figure, each set of data exhibits an excellent linear relationship. The slope of the lines corresponds to the true hardness (H_0) when the intercept of the lines denotes the surface energy (γ) value. The H_0, γ and *LRC* values

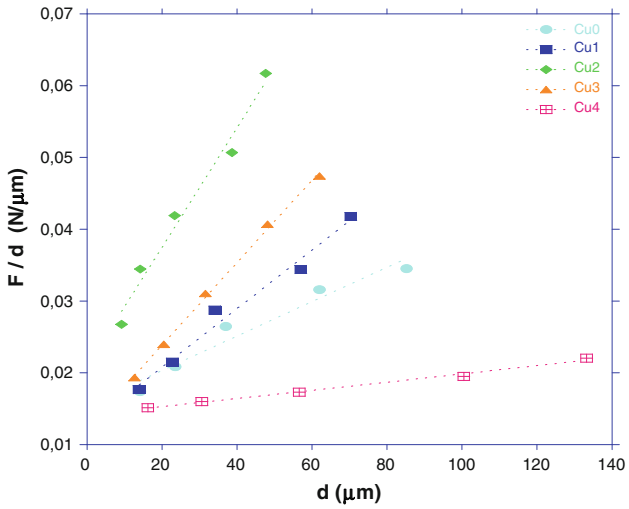

Fig. 9 *Plots* of *F*/*d* versus *d* for the samples

Table 6 Best-fit results of experimental data according to Eq. 12

Samples	H_0 (GPa)	γ (N/µm)	LRC	H_v (GPa)
Cu0	0.444	0.015	0.9749	0.751–0.945
Cu1	0.756	0.012	0.9896	1.102–1.119
Cu2	1.542	0.021	0.9895	2.402–2.429
Cu3	1.065	0.013	0.9988	1.417–1.568
Cu4	0.106	0.014	0.9959	0.307–0.360

obtained are listed in Table 6. It is clear from the table that when the true hardness and surface energy values enhance with the increase in the annealing time up to 1 h, these parameters tend to decrease for the Cu3 and Cu4 sample. Similar to the Vickers microhardness results, the minimum values are observed for the Cu4 sample.

Additionally, the load independent values of the elastic modulus (E_0), yield strength (Y_0), fracture toughness (K_{IC}) and brittleness index (B_0) of the samples, calculated with aid of the true microhardness (load independent, H_0), are given in Table 7. According to the table, all the E_0, Y_0, K_{IC} and B_0 values obtained enhance with the decrement in the applied loads; on the other hand, the E_0, Y_0, K_{IC} and B_0 values increase with ascending the diffusion-annealing time up to 1 h but they decrease for the Cu3 and Cu4 sample. In fact the minimum values are observed for the

Table 7 The calculated load independent H_0, E_0, Y_0 and K_{IC} for the samples

Samples	H_0 (GPa)	E_0 (GPa)	Y_0 (GPa)	K_{IC} (Pa/m$^{1/2}$)	B_0 (µm$^{1/2}$)	H_v (GPa)
Cu0	0.444	36.39	0.148	1.062	0.418	0.751–0.945
Cu1	0.756	61.96	0.252	1.249	0.605	1.102–1.119
Cu2	1.542	126.38	0.514	2.298	0.671	2.402–2.429
Cu3	1.065	87.29	0.355	1.483	0.618	1.417–1.568
Cu4	0.106	8.68	0.035	0.494	0.214	0.307–0.360

Cu4 sample. Based on the results, the load independent values obtained for all the samples are found to be closer to the experimentally estimated values in the plateau region, compared to the load dependent values. As a result, the energy dissipation method allows us to investigate the behavior of the samples in the plateau region rather than the elastic portion method. The similar results were also observed in the literature [31, 35, 36].

4 Conclusion

In this study, the influence of the different annealing time (0.5, 1, 1.5 and 2 h) on the microstructural, superconducting and mechanical properties of the Cu diffused bulk MgB_2 superconductor with the aid of the dc resistivity, X-ray diffraction, scanning electron microscopy and Vickers microhardness measurements. The results obtained demonstrate that the microstructural, superconducting and mechanical properties of the bulk MgB_2 superconductors produced depend strongly on the annealing time and following findings are concluded:

- Both the onset and offset transition temperature increase with the enhancement in the diffusion-annealing time up to 1 h after which they start to decrease.
- According to results of XRD and SEM investigations, the Cu2 sample obtaining the largest lattice parameters shows the best surface morphology, best grain connectivity, largest grain size and lowest porosity among the samples.
- The maximum diffusion coefficient is obtained to be about 2.58×10^{-7} cm^2 s^{-1} for the Cu2 sample.
- The Vickers microhardness values of all the samples studied show the typical ISE behavior. The Vickers microhardness, elastic modulus, yield strength, fracture toughness and brittleness index values decrease with the increase in the applied load. Moreover, the load independent microhardness (H_0), elastic modulus (E_0), yield strength (Y_0) fracture toughness (K_{IC}) and brittleness index (B_0) are found to be lower than load dependent values (H_v, E, Y, K_{IC} and B), confirming that the energy dissipation method examining the behavior of the samples in the plateau region is superior to the elastic portion method.

References

1. J. Nagamatsu, N. Nakagawa, T. Muranaka, Y. Zenitani, J. Akimitsu, Nature **410**, 63 (2001)
2. C. Buzea, T. Yamashita, Supercond. Sci. Technol. **14**, R115 (2001)
3. K. Vinod, R.G.A. Kumar, U. Syamaprasad, Supercond. Sci. Technol. **20**, R1 (2007)
4. S. Altin, M.A. Aksan, M.E. Yakinci, J. Phys. Chem. Solids. **72**, 1070 (2011)
5. N.K. Kim, K.S. Tan, B.H. Jun, H.W. Park, J. Joo, C.J. Kim, Phys. C. **468**, 1375 (2008)
6. A. Yamamoto, J.I. Shimoyama, S. Ueda, Y. Katsura, S. Horii, K. Kishio, Supercond. Sci. Technol. **17**, 921 (2004)
7. S. Zhou, S. Dou, Solid State Sci. **12**, 105 (2010)
8. Q. Cai, Y. Liu, Z. Ma, Z. Dong, J. Supercond. Nov. Magn. **25**, 357 (2012)
9. E.T. Koparan, A. Surdu, A. Sidorenko, E. Yanmaz, Phys. C. **473**, 1 (2012)
10. N.N. Kolesnikov, M.P. Kulakov, Phys. C. **363**, 166 (2001)
11. X.F. Pan, Y. Zhao, Y. Feng, Y. Yang, C.H. Cheng, Phys. C. **468**, 1169 (2008)
12. Z. Ma, Y. Liu, Mater. Chem. Phys. **126**, 114 (2011)
13. Y. Zhang, S.H. Zhou, X.L. Wang, S.X. Dou, Phys. C. **468**, 1383 (2008)
14. M. Dogruer, G. Yildirim, E. Yucel, C. Terzioglu, J. Mater. Sci. Mater. Electron. (2012). doi:10.1007/s10854-012-0689-6
15. M. Yilmazlar, O. Ozturk, O. Gorur, I. Belenli, C. Terzioglu, Supercond. Sci. Tech. **20**, 365 (2007)
16. B.D. Cullity, *Elemt of X-ray diffraction*, 3rd edn. (Addition-Wesley, Reading, 2001)
17. G. Yildirim, E. Yucel, S. Bal, M. Dogruer, A. Varilci, M. Akdogan, C. Terzioglu, Y. Zalaoglu, J. Supercond. Nov. Magn. **25**, 231 (2012)
18. A. Ianculescu, M. Gartner, B. Despax, V. Bley, Th. Gavrila, R. Leby, M. Modreanu, Appl. Surf. Sci. **253**, 344 (1996)
19. J. Napieralski, A. Kryza, J. Kasperczyk, I.V. Kityk, J. Phys. Chem. Solids. **62**, 1949 (2001)
20. J. Economy, R. Anderson, Inorg. Chem. **5**, 989 (1966)
21. C. Terzioglu, H. Aydin, O. Ozturk, E. Bekiroglu, I. Belenli, Phys. B. **403**, 3354 (2008)
22. G. Yildirim, S. Bal, E. Yucel, M. Dogruer, M. Akdogan, A. Varilci, C. Terzioglu, J. Supercond. Nov. Magn. **25**, 381 (2012)
23. C. Terzioglu, Phys. B. **403**, 3320 (2008)
24. C. Terzioglu, O. Ozturk, I. Belenli, J. Alloys Comp. **471**, 142 (2009)
25. O. Ozturk, H.A. Cetinkara, E. Asikuzun, M. Akdogan, M. Yilmazlar, C. Terzioglu, J. Mater. Sci. Mater. Electron. **22**, 1501 (2011)
26. E. Asikuzun, O. Ozturk, H.A. Cetinkara, G. Yildirim, A. Varilci, M. Yılmazlar, C. Terzioglu, J. Mater. Sci. Mater. Electron. (2011). doi:10.1007/s10854-011-0537-0
27. H.C. Ling, M.F. Yan, J. Appl. Phys. **64**, 1307 (1988)
28. U. Kolemen, O. Uzun, M.A. Aksan, N. Guc lu, E. Yakıncı, J. Alloys Comp. **415**, 294 (2006)
29. S.M. Khalil, J. Phys. Chem. Solids. **62**, 457 (2001)
30. Z. Li, A. Ghosh, A.S. Kobayashi, J. Am. Ceram. Soc. **72**, 904 (1989)
31. J.B. Quinn, G.D. Quinn, J. Mater. Sci. **31**, 4331 (1997)
32. N.H. Mohammed, A.I. Abou-Aly, I.H. Ibrahim, R. Awad, M. Rekaby, J. Supercond. Nov. Magn. **24**, 1463 (2011)
33. A. Leenders, M. Mich, H.C. Freyhard, Phys. C **279**, 173 (1997)
34. K. Hirao, M. Tomozawa, J. Am. Ceram. Soc. **70**, 497 (1987)
35. R. Tickoo, R.P. Tandon, K.K. Bamzai, P.N. Kotru, Mater. Chem. Phys. **80**, 446 (2003)
36. A.A. Elmustafa, D.S. Stone, J. Mech. Phys. Solids. **51**, 357 (2003)